

Article

Predicting Stem Total and Assortment Volumes in an Industrial *Pinus taeda* L. Forest Plantation Using Airborne Laser Scanning Data and Random Forest

Carlos Alberto Silva ^{1,2,3,*}, Carine Klauberg ², Andrew Thomas Hudak ², Lee Alexander Vierling ¹, Wan Shafrina Wan Mohd Jaafar ⁴, Midhun Mohan ⁵, Mariano Garcia ⁶ , António Ferraz ³, Adrián Cardil ⁷ and Sassan Saatchi ³

¹ Department of Natural Resources and Society, College of Natural Resources, University of Idaho (UI), 875 Perimeter Drive, Moscow, ID 83843, USA; leev@uidaho.edu

² US Forest Service (USDA), Rocky Mountain Research Station, RMRS, 1221 South Main Street, Moscow, ID 83843, USA; carine_klauberg@hotmail.com (C.K.); ahudak@fs.fes.us (A.T.H.)

³ Jet Propulsion Laboratory, California Institute of Technology 4800 Oak Grove Drive, Pasadena, CA 91109, USA; ferraz.antonio.a@gmail.com (A.F.); sasan.s.saatchi@jpl.nasa.gov (S.S.)

⁴ School of Geosciences, University of Edinburgh, Edinburgh EH8 9XL, UK; wanshafrina@gmail.com

⁵ Department of Forestry and Environmental Resources, North Carolina State University, 2800 Faucette Drive, Raleigh, NC 27695, USA; mmohan2@ncsu.edu

⁶ Centre for Landscape and Climate Research, Department of Geography, University of Leicester, Leicester LE1 7RH, UK; mariano.gar.alo@gmail.com

⁷ Tecnosylva Parque Tecnológico de León, 24009 León, Spain; adriancardil@gmail.com

* Correspondence: carlos_engflorestal@outlook.com; Tel.: +1-(208)-5964510

Academic Editor: Timothy A. Martin

Received: 27 April 2017; Accepted: 13 July 2017; Published: 17 July 2017

Abstract: Improvements in the management of pine plantations result in multiple industrial and environmental benefits. Remote sensing techniques can dramatically increase the efficiency of plantation management by reducing or replacing time-consuming field sampling. We tested the utility and accuracy of combining field and airborne lidar data with Random Forest, a supervised machine learning algorithm, to estimate stem total and assortment (commercial and pulpwood) volumes in an industrial *Pinus taeda* L. forest plantation in southern Brazil. Random Forest was populated using field and lidar-derived forest metrics from 50 sample plots with trees ranging from three to nine years old. We found that a model defined as a function of only two metrics (height of the top of the canopy and the skewness of the vertical distribution of lidar points) has a very strong and unbiased predictive power. We found that predictions of total, commercial, and pulp volume, respectively, showed an adjusted R^2 equal to 0.98, 0.98 and 0.96, with unbiased predictions of -0.17% , -0.12% and -0.23% , and Root Mean Square Error (RMSE) values of 7.83%, 7.71% and 8.63%. Our methodology makes use of commercially available airborne lidar and widely used mathematical tools to provide solutions for increasing the industry efficiency in monitoring and managing wood volume.

Keywords: forest inventory; lidar; remote sensing; supply chain

1. Introduction

The area of planted forests worldwide has been steadily growing, with an estimated 6.95% of total global forested area being plantations in 2010 [1]. Tropical regions may be experiencing particularly rapid rates of plantation expansion [2]. For example, the area of pine plantations in Brazil has dramatically risen in the last few decades to increase pulp and paper production. Currently ~20% of the total reforested area of Brazil is comprised of pine forest plantations [2].

Most of the pine plantations are concentrated in South Brazil, with 34.1% and 42.4% of the total reforested area located in Paraná and Santa Catarina states [2]. *Pinus taeda* L., also known as loblolly pine, is the most planted forest specie in these regions. It has high economic importance due to its high volumetric increment in the colder regions of the southern Brazil [3]. It has fast growing rates presenting increments up to $50 \text{ m}^3 \cdot \text{ha}^{-1} \cdot \text{year}^{-1}$ [2]. Moreover, *P. taeda* is commonly managed for production of multiple types of wood such as stem total, saw logs, pulpwood and small-diameter logs and branches, which are used for energy. Saw logs and pulpwood can be further divided into different assortments that differ in size and therefore in economic value [3].

Forest inventory in *P. taeda* is currently based on field measurements and typically conducted annually to monitor forest growth in Brazil, allowing managers to identify problematic conditions during initial growth stages, and determine optimal harvest time [4]. While field measurements are considered the most accurate approach for monitoring industrial forest plantations, measuring stem total and assortment volumes annually via traditional methods is an extremely time consuming and labor-intensive task, especially in large plantations where a huge number of plots need to be measured to characterize the variation [5]. Hence, to improve plantation management there is a need to develop and implement accurate, repeatable, and economical remote sensing based methods that provide synoptic coverage at high spatial resolution.

Over the past few decades, lidar remote sensing has been established as one of the promising and primary tools for broad-scale analysis of forest systems. Lidar data can be used to characterize local to regional spatial extents with high enough resolution to quantify the three-dimensional structure of the forest with the support of efficiently collected field data and several statistical methods (e.g., [6–10]). Lidar can be used to produce highly accurate retrievals of tree density, stem total and assortment volumes, basal area, aboveground carbon, and leaf area index, and thereby can be an effective way to predict and map forest attributes at unsampled locations (e.g., [11–16]). To parlay these attributes into improved forest management practices for wood and pulp production, it is often necessary to predict stem total and assortment volumes of pine plantations in operational and experimental scenarios, as these scenarios often include thinning cruises, mid-rotation cruises, genetic trials, and silviculture research tests [17].

Current predictive modeling methods include parametric (e.g., multiple linear regression) and non-parametric (e.g., Random Forest) approaches (e.g., [6,7,18]). Among the machine learning algorithms, the Random Forest (RF) modeling approach has gained popularity in estimating forest attributes from lidar data due to its flexibility and ability to maintain nonlinear dependences compared to parametric algorithms [19]. The RF can be viewed as an improved version of classification and regression tree (CART) methods; data and variables can be randomly sampled by RF in an iterative bagging bootstrap procedure to generate a “forest” of regression trees [20]. Also, incorporation of multiple decision trees and internal cross-validation has improved results, enhanced ease of use and reduced issues regarding over-fitting while performing this modeling approach [21,22]. In case of regression-type problems, RF acts as an arbitrary number of simple trees whose responses are averaged to obtain an estimate of dependent variables [23]. Diversification of sample trees is primarily done in two ways, either through a balancing methodology where equal numbers of samples are drawn from minority classes and majority classes, or by assigning a higher weight (i.e., heavier penalty) on misclassified minority class and taking the majority voting of individual classification trees [24]. As RF does not require any assumptions about the relationships between explanatory and response variables, they are considered well suited for analyzing complex non-linear and possibly hierarchical interactions in large datasets [25]. In forest inventory, RF has been used for predicting and mapping forest attribute at the stand (e.g., [19]) and individual tree levels [23], in addition to disturbance evaluation (e.g., [26]), mapping invasive plant species (e.g., [27]), and vegetation classification (e.g., [21]). Despite of the above-mentioned studies, to our knowledge, lidar and RF have been not yet been combined for predicting and mapping stem total, saw log and pulpwood volumes in industrial *P. taeda* forest plantations at stand level.

Timely monitoring of stem total and assortment volumes in *P. taeda* plantations with lidar data and RF would allow managers to determine the optimal time for harvest or other treatment activities

to maximize economic return. Therefore, the development of robust frameworks for modeling and mapping stem total and assortment volumes at plot and stand levels is still needed to increase the efficiency in monitoring and managing wood and pulp productions in forest plantations. Moreover, efficient frameworks also play important role in helping lidar technology move from research to operational modes, especially in industrial forest plantation settings where lidar applications are relatively new. The aims of this study were to: (i) present a robust and efficient framework for modeling, predicting and mapping stem total volume (V_t), saw logs (in this study mentioned as commercial) volume (V_c) and pulpwood volume (V_p) in a *P. taeda* plantation in southern Brazil using airborne lidar data; (ii) evaluate the use of the RF machine learning algorithm for modeling stem total and assortment volumes; and (iii) generate maps representing the spatial distribution of V_t , V_c and V_p in differently aged plantations of *P. taeda*. This investigation was based on the hypothesis that lidar technology and Random Forest analysis can facilitate accurate and precise inferences of forest volumes in *P. taeda* plantations in southern Brazil.

2. Methods

2.1. Study Area Description

The study area consisted of *P. taeda* stands located within the Telémaco Borba municipality in the state of Paraná, southern of Brazil (Figure 1). Trees were planted using a 3.0×2.0 m or 2.5×2.5 m grid configuration, resulting in an average tree density of 1667 or 2000 trees ha^{-1} , respectively. The climate of the region is characterized as warm and temperate [28], with annual average precipitation of approximately 1378 mm and an annual average temperature of 18.4 °C. The *P. taeda* stands are situated on a plateau where the topography is relatively flat. The plantations are managed by Klabin S.A., a pulp and paper company.

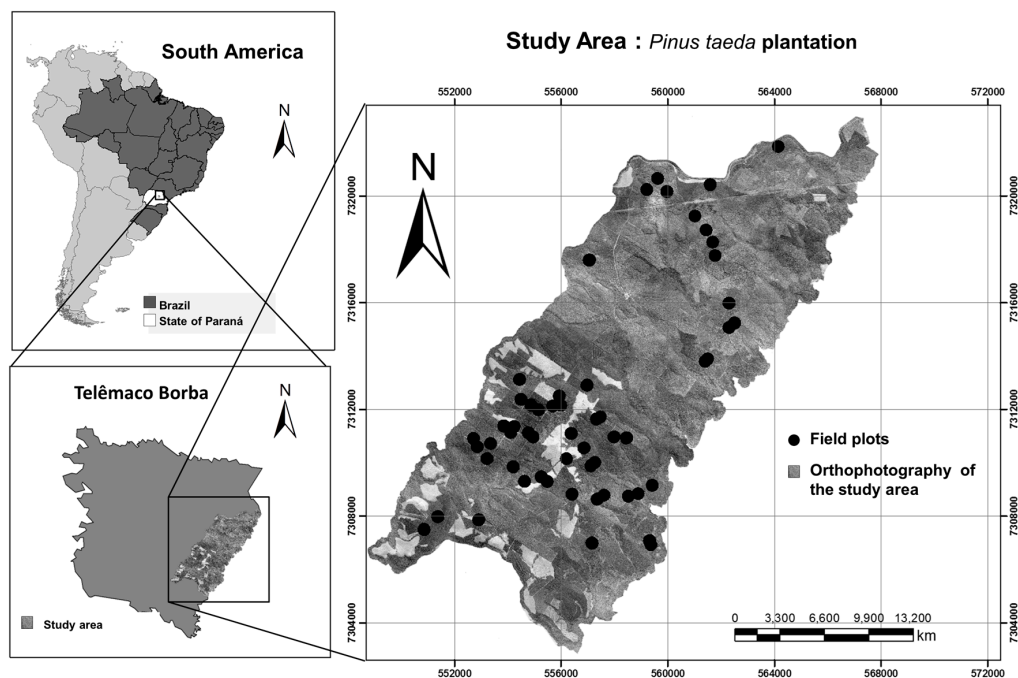


Figure 1. Location of study area in Telémaco Borba, Paraná, Brazil. The black dots indicate the location of the *Pinus taeda* stands.

2.2. Field Data Collection

A total of 50 rectangular plots, each approximately 600 m^2 (i.e., 20 m \times 30 m) were randomly established and measured across 50 stands distributed in four plantations. As such, the sample plots

well represent the study area, and they capture the entire structural variability in these stands with ages ranging from three to nine years old. All plots were geo-referenced with a geodetic GPS with differential correction capability (Trimble Pro-XR, Trimble, Sunnyvale, CA, USA) ensuring a location error lower than 10 cm. In each sample plot, individual trees were measured for dbh (diameter at breast height) at 1.30 m and a random subsample (15%) of trees for tree height (Ht). For those trees in the plots that were not directly measured for Ht, the inventory team of Klabin S.A. predicted heights from hypsometric equations [29], employing dbh as the independent variable, and Ht as the dependent variable, following the model below:

$$\ln(Ht) = \beta_0 + \beta_1 \times (1/dbh) + e \tag{1}$$

where $\ln(Ht)$ is the natural logarithm of tree height (m); β_0 and β_1 are the intercept and the slope of the model; dbh is the diameter at breast height (1.30 m) and e is the random error of the model. The coefficients of the hypsometric models are the companies intellectual property and not made available to the public, however, the adjusted coefficient of determination (adj. R^2) and standard error of estimate in percentage (SEE%) of the models ranged from 0.96 to 0.98 and 5.1 to 6.5, respectively.

The management goal of the *P. taeda* plantations at Klabin is optimized to produce commercial logs of 2.65 m in length, which are then classified in four timber assortment classes: 18 to 25 cm (Vc 1), 25 to 30 cm (Vc 2), 30 to 40 cm (Vc 3), and diameter ≥ 40 cm (Vc 4). The logs designated for pulpwood are produced with log lengths of 2.40 m and diameters ranging from 8 to 18 cm (Vp), as illustrated in Figure 2.

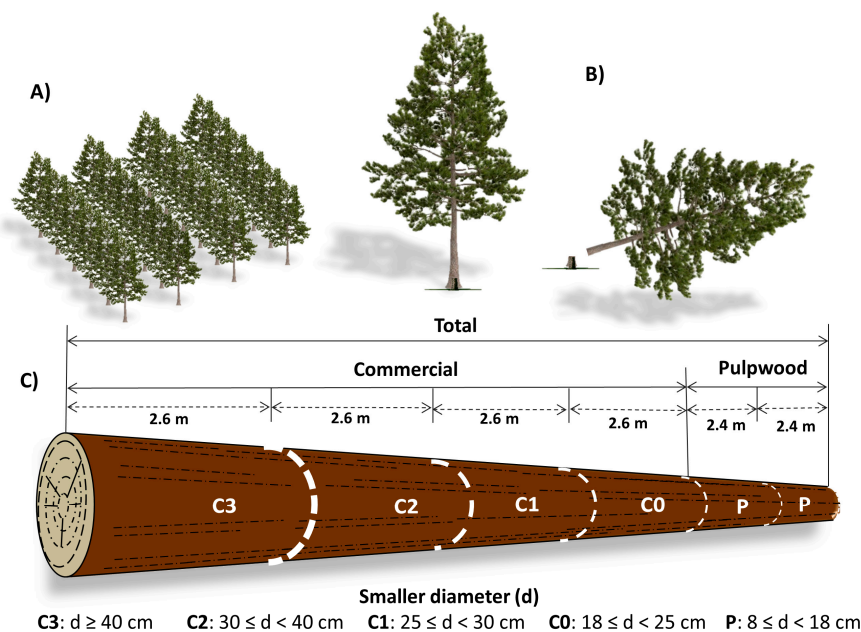


Figure 2. Process of forest volume measurement. (A) *Pinus* plantation; (B) Timber harvester and (C) Log segmentation for classes of volume measurements.

In this study, V_t , V_c and V_p for each tree were computed using the fifth-degree polynomial [30] as presented below:

$$\frac{d_i}{dbh} = \left[\beta_0 + \beta_1 \left(\frac{h_i}{h} \right) + \beta_2 \left(\frac{h_i}{h} \right)^2 + \beta_3 \left(\frac{h_i}{h} \right)^3 + \beta_4 \left(\frac{h_i}{h} \right)^4 + \beta_5 \left(\frac{h_i}{h} \right)^5 \right] \tag{2}$$

$$V = K \int_{h_1}^{h_2} d_i^2 \delta h \tag{3}$$

$$V = K \text{ dbh}^2 \int_{h_1}^{h_2} (\beta_0 + \beta_1/h \times h_1^1 + \beta_2/h^2 \times h_2^2 + \beta_3/h^3 \times h_2^3 + \beta_4/h^4 \times h_2^4 + \beta_5/h^5 \times h_2^5)^2 \delta h \quad (4)$$

where β = parameters to be estimated; d_i = stem diameter (cm) at the i th position; dbh = diameter (cm) at breast height (1.30 m); h = total height (m); h_i = height (m) at the i th position; and $K = \pi/40,000$ is an adjustment factor to estimate volume as $\text{m}^3 \cdot \text{ha}^{-1}$.

The polynomial models were adjusted for classes of dbh, and the coefficients of the models are the companies' intellectual property and not made available to the public; however, the classes of diameter, adj. R^2 and standard error of the estimate (SEE; given in %) for the polynomial models used in this study are presented in Table 1.

Table 1. Statistics of the taper models.

DBH (cm) Range	Adj. R^2	SEE (%)	
		dbh	Volume
0.0–17.9	0.96	9.58	11.55
18.0–29.9	0.98	7.99	9.33
30.0–70.0	0.98	7.52	8.21

The total of V_t , V_c and V_p of all individuals were summed at plot-level and scaled to a hectare. The summary of volumes in $\text{m}^3 \cdot \text{ha}^{-1}$ for each class of stand ages is presented in Table 2. SEE (%) is the standard error of the estimate, expressed as a percentage.

Table 2. Summary of stem volumes computed in the 50 field sample plots.

Ages (I)	Stem Total and Assortment Volumes ($\text{m}^3 \cdot \text{ha}^{-1}$)			N
	V_t	V_c	V_p	
$3 \leq I < 5$	56.25 ± 10.98	47.53 ± 12.15	45.67 ± 11.14	19
$5 \leq I < 7$	134.20 ± 30.77	124.67 ± 30.3	114.20 ± 23.41	22
$7 \leq I < 9$	169.50 ± 22.86	160.2 ± 22.20	129.50 ± 24.83	13
Mean \pm Sd	113.70 ± 52.53	103.86 ± 52.99	92.13 ± 42.11	Total = 50

N = number of plots.

2.3. Lidar Data Acquisition and Data Processing

Lidar data were obtained by a Harrier 68i sensor (Trimble, Sunnyvale, CA, USA) mounted on a CESSNA 206 aircraft. The characteristics of the lidar data acquisition are listed in Table 3. Lidar data processing consisted of several steps that ingested the lidar point cloud data and provided two major outputs: the digital terrain model (DTM), and the lidar-derived canopy structure metrics. All lidar processing was performed using FUSION/LDV 3.42 software (US Forest Service, Washington, DC, USA) [31].

Table 3. Airborne lidar system characteristics.

Parameter	Value
Scan angle ($^\circ$)	$\pm 30^\circ$
Footprint (m)	0.33 m
Flight speed (km/h)	234.0 km/h
Horizontal accuracy	10 cm
Elevation accuracy	15 cm
Operating altitude	666.17 m
Scan frequency	300 kHz
Pulse density	4 pulse m^{-2}

The original point cloud data were filtered using Kraus and Pfeifer’s algorithm [32] and a 1 m resolution DTM was generated from the points classified as ground. Subsequently, the height of the returns was computed by subtracting the elevation of the DTM from each return. Once the heights were normalized, the metrics shown in Table 4 were computed at plot and stand levels, at a grid cell resolution of 25 m, using all lidar returns.

Table 4. Lidar-derived canopy height metrics considered as candidate variables for predictive V models [31].

Variable	Description
HMIN	Height Minimum
HMAX	Height Maximum
HMEAN	Height Mean
HMAD	Height median absolute deviation
HSD	Height standard deviation
HSKEW	Height skewness
HKURT	Height kurtosis
HCV	Height coefficient of variation
HIQ	Height interquartile range
HMODE	Height mode
H01TH	Height 1th percentile
H05TH	Height 5th percentile
H10TH	Height 10th percentile
H15TH	Height 15th percentile
H20TH	Height 20th percentile
H25TH	Height 25th percentile
H30TH	Height 30th percentile
H35TH	Height 35th percentile
H40TH	Height 40th percentile
H45TH	Height 45th percentile
H50TH	Height 50th percentile
H55TH	Height 55th percentile
H60TH	Height 60th percentile
H65TH	Height 65th percentile
H70TH	Height 70th percentile
H75TH	Height 75th percentile
H80TH	Height 80th percentile
H90TH	Height 90th percentile
H95TH	Height 95th percentile
H99TH	Height 99th percentile
CR	Canopy Relief Ratio $((HMEAN - HMIN)/(HMAX - HMIN))$
COV	Canopy Cover (Percentage of first return above 1.30 m)

2.4. Predictor Variables Selection

In order to derived accurate estimates of stem volumes from lidar, it is essential to select the most significant lidar metrics (predictor variables) for modeling within a parsimonious statistical model framework. Because the number of candidate lidar metrics can be very large (e.g., 30 metrics), in our study we selected the best lidar metrics for modeling stem volumes based on two steps. First, even though highly correlated variables will not cause multi-collinearity issues in RF [20], Pearson’s correlation (r) was used to identify highly correlated predictor variables ($r > 0.9$) as presented in previous studies (e.g., [14,33,34]). If a given group (2 or more) of lidar metrics were highly correlated, we retained only one metric by excluding the others that were most highly correlated with the remaining metrics. Second, we identified the most important metrics based on the Model Improvement Ratio (MIR), a standardized measure of variable importance [35,36]. MIR scores are derived by dividing raw variable important scores (output from RF models) by the maximum variable importance score, so that MIR values range from 0 to 1. MIR scores allow for variable importance comparisons among

different RF models. We ran the RF routine (package randomForest [37]) in R [38] 1000 times to compute MIR. In each MIR iteration, we bootstrapped the data by randomly selecting a sample of 50 plots with replacement. RF requires two parameters to be set: (i) mtry, the number of predictor variables performing the data partitioning at each node which in this study was defined by the number of highly uncorrelated preliminary set of lidar metrics and (ii) ntree, the total number of trees to be grown in the model run which was set to 1000 (e.g., [34,39]). Running 1000 iterations of RF produced consistent MIR distributions and avoided unnecessary processing time [39]. To create parsimonious models, we reserved the metrics for final RF models that exhibited the highest mean MIR values.

2.5. Random Forest Model Development

The three stem volumes (Vt, Vc and Vp) of interest were predicted at the plot and stand-levels using also the RF package [37] in R [38]. The number of RF trees to grow was set to 1000, and the number of predictor variables performing the data partitioning at each node was set to equal the number of best lidar metrics selected by MIR on Section 2.4 [37]. The accuracy of estimates for each model was evaluated in terms of Adj. R^2 , Root Mean Square Error (RMSE), and Bias (both absolute and relative) by the linear relationship between predicted (output from RF) and observed stem volumes:

$$\text{RMSE (m}^3 \cdot \text{ha}^{-1}) = \sqrt{\sum_{i=1}^n (y_i - \hat{y}_i)^2 / n} \quad (5)$$

$$\text{Bias (m}^3 \cdot \text{ha}^{-1}) = \frac{1}{n} \sum_{i=1}^n (y_i - \hat{y}_i) \quad (6)$$

where n is the number of plots, y_i is the observed value for plot i , and \hat{y}_i is the predicted value for plot i . Moreover, relative RMSE (%) and biases (%) were calculated by dividing the absolute values (Equations (5) and (6)) by the mean of the observed stem volume. Based on earlier experiences and recommendations from literature [4,5], we defined acceptable model accuracy as a relative RMSE and Bias of <15%.

For validation purposes, RF models were embedded in a bootstrap with 500 iterations. In each bootstrap iteration, we drew 50 times with replacement from the 50 available samples. In this procedure, on average 44% of the total of sample (~22 samples) are not drawn. These samples were subsequently used as holdout samples for an independent validation (e.g., [40]). In each bootstrap iteration, Adj. R^2 , absolute and relative RMSE and Bias were computed based on the linear relationship between observed and predicted volumes using the holdout samples. We used also two-sided Kolmogorov-Smirnov (KS) in R [38] and a statistical equivalence test [41] to compare the field- and lidar-based stem volume estimates in each iteration.

2.6. Predictive Stem Volumes Maps

Predictive maps of stem volumes at 25 m of spatial resolution were generated based on the RF models containing the best lidar metrics according to MIR analysis. Because we have a large number of stands in this study, stem volumes predictions at the stand level were then presented herein by stand ages of 3–5, 5–7 and 7–9 years. Additionally, maps of coefficient of variation (CV, given in %) values for the stem volume predictions (as obtained from the 500 bootstrap runs) was also produced for each stand (e.g., [40]). Figure 3 provides an overview of the study methodology.

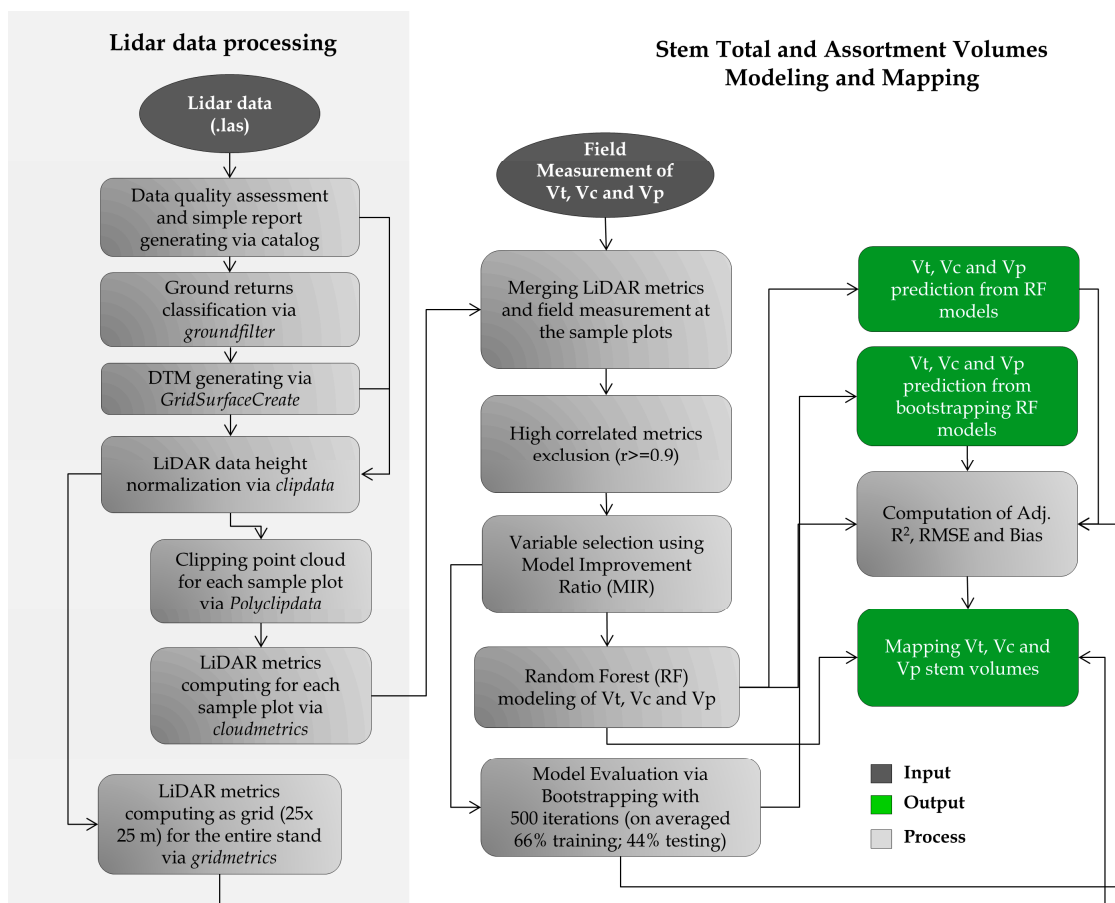


Figure 3. Procedure for predicting stem total and assortment volumes in an industrial *P. taeda* forest plantation using airborne laser scanning data and random forest.

3. Results

3.1. Predictor Variable Selection

A total of 25 of the 32 lidar metrics showed a very strong correlation ($r > 0.9$). We retained one of the highly correlated metrics (H99TH), which along with seven other remaining metrics not extremely highly correlated ($r \geq 0.9$) were included in the MIR analysis (Table 5). LiDAR metrics that were retained after correlation analysis included HMIN, HCV, HIQ, HSKEW, HKUR, H99TH and COV. Among these, H99TH and HSKEW exhibited the highest mean MIR values (Table 6) and therefore, were used for model development. Although HCV also showed high mean MIR values, its inclusion in the models did not significantly improve model performance.

Table 5. Pearson’s correlations among lidar metrics selected.

<i>r</i>	HMIN	HCV	HIQ	HSKEW	HKUR	H99TH	COV
HCV	−0.45 **						
HIQ	0.14	−0.09					
HSKEW	−0.30 **	0.83 ***	−0.36 *				
HKUR	0.27	−0.81 ***	0.07	−0.82 ***			
H99TH	0.39 **	−0.80 ***	0.61 ***	−0.81 ***	0.77 ***		
COV	0.23	−0.74 ***	0.12	−0.67 ***	0.53 ***	0.58 ***	

“***”: p -value < 0.001; “**”: p -value < 0.01; “*”: p -value < 0.05; If there is no *: p -value \geq 0.05.

Table 6. Mean of the model improvement ratio (MIR) among the remained lidar-derived metrics not highly correlated. The bold represents the highest MIR values.

Attributes	LiDAR-Derived Metrics						
	HMIN	HCV	HIQ	HSKEW	HKUR	H99TH	COV
Vt	0.16	0.40	0.18	0.75	0.31	0.99	0.12
Vc	0.15	0.39	0.17	0.77	0.30	0.99	0.10
Vp	0.16	0.65	0.20	0.74	0.38	0.98	0.11

3.2. Model Performances

The H99TH and HSKEW that exhibited high MIR values explained more than 80% variations of the stem volumes in Vt, Vc and Vp components with relative RMSE and Bias less than 10% and -0.10% , respectively (Table 7). The negative values in Bias indicate that the models are slightly underestimating the stem volumes. Predicted stem volumes at plot level did not differ significantly to the observed stem volumes by the KS and equivalence tests (p -values > 0.05). Figure 4 shows the distribution of observed and stem volumes and a good agreement can be observed.

Table 7. Model accuracies of random forest (RF) models per stem volume in terms of Adj. R^2 , Root Mean Square Error (RMSE) and bias calculated by the relationship between predicted and observed stem volumes.

Volume	LiDAR Derived Metrics	Adj. R^2	RMSE		Bias	
			$\text{m}^3 \cdot \text{ha}^{-1}$	%	$\text{m}^3 \cdot \text{ha}^{-1}$	%
Vt	H99TH + HSKEW	0.97	8.91	7.83	-0.19	-0.17
Vc		0.98	8.00	7.71	-0.12	-0.12
Vp		0.96	7.96	8.63	-0.22	-0.24

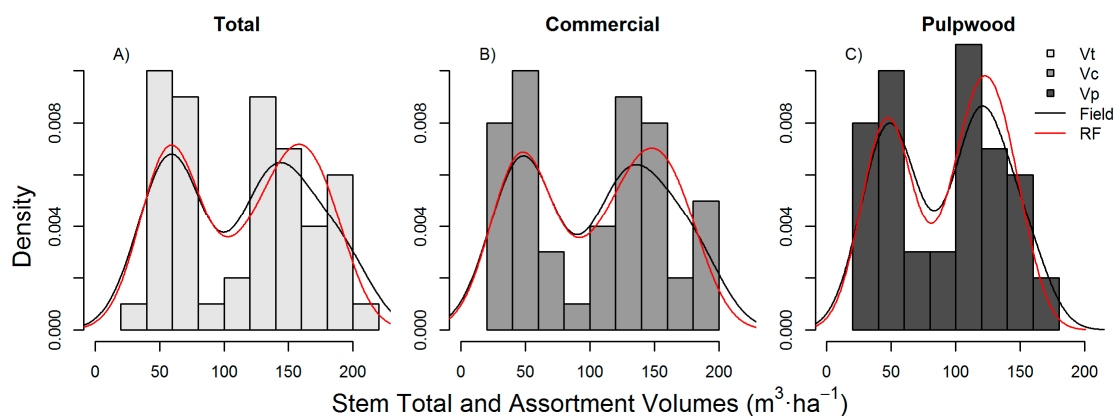


Figure 4. Distribution of observed (black line) and predicted (red line) stem volume from RF. The gray histograms is based from field data. (A) Total volume (Vt) (B) Commercial volume (Vc) and (C) Pulpwood volume (Vp).

The performance of RF model to predict Vt, Vc and Vp was also summarized in terms of Adj. R^2 , RMSE and Bias for all 500 bootstrap runs (Table 8). Observed and predicted stem volumes in each bootstrap iteration did not differ significantly by the statistical KS and equivalence test (p -values > 0.05) as well. Overall, all models using H99TH and HSKEW performed very well, with relative RMSE and Bias $< 15\%$ in the bootstrap procedure. The observed and the average of the predicted stem volumes from the 500 bootstrap runs were also compared and according to the KS and equivalence tests those values did not differ significantly (p -values > 0.05) too (Figure 5).

Table 8. Model accuracies per stem volume type. The average and standard deviation of Adj. R^2 , RMSE and bias derived from the 500 bootstrap runs are displayed.

Volume	Adj. R^2	RMSE		Bias	
		$\text{m}^3 \cdot \text{ha}^{-1}$	%	$\text{m}^3 \cdot \text{ha}^{-1}$	%
Vt	0.94 ± 0.02	12.02 ± 2.78	9.80 ± 2.18	-0.58 ± 2.85	-0.45 ± 2.30
Vc	0.95 ± 0.02	11.67 ± 2.76	10.31 ± 2.76	-0.95 ± 2.80	-0.82 ± 2.45
Vp	0.91 ± 0.04	11.83 ± 2.56	12.10 ± 2.57	-0.49 ± 2.73	-0.54 ± 2.77

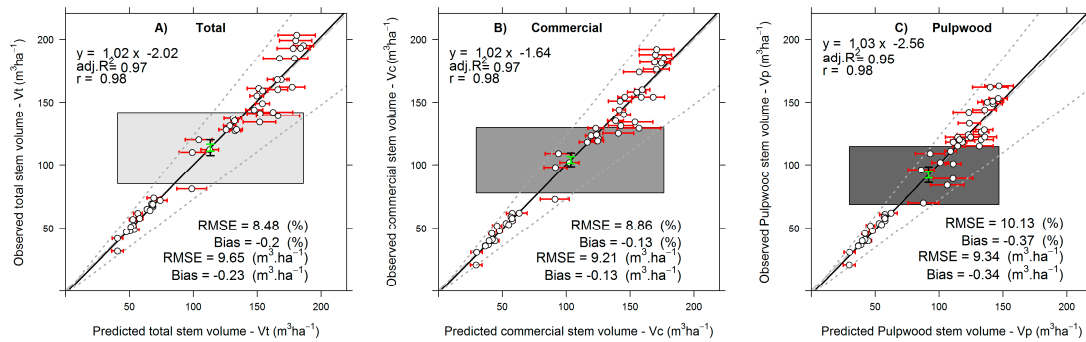


Figure 5. Equivalence plots of the observed and the mean of predicted Vt (A), Vc (B) and Vp (C) obtained from the 500 bootstrapped RF model runs. ($N = 50$). The equivalence plot design presented herein is an adaptation of the original equivalence plots presented by [41]. The grey polygon represents the $\pm 25\%$ region of equivalence for the intercept, and the green vertical bar represents a 95% of confidence interval for the intercept. The predicted stem volumes from the RF models are equivalent with reference to the intercept and slope since the green bar is completely within the grey polygon. If the grey polygon is lower than the green vertical bar, the predicted stem volumes are negatively biased; and if it is higher than the green vertical bar, the predicted stem volumes are positively biased. Moreover, the grey dashed line represents the $\pm 25\%$ region of equivalence for the slope, the fit line is within the dotted lines and the black vertical bar is within the gray rectangle, indicating that the pairwise measurements are equivalent. A green bar that is wider than the region outlined by the grey dashed lines indicates highly variable predictions. The white dots are the pairwise measurements, and the solid line is a best-fit linear model for the pairwise measurements. The light grey dashed line represented the relationship 1:1. The horizontal red bars represent the standard deviation of the 500 bootstrapping predictions.

3.3. Prediction Maps

Box plots of predicted stem values of Vt, Vc and Vp of *P. taeda* at the stand level are shown in Figure 5. On average, naturally predicted stem volumes tended to be lower at young age (Figure 6A) and higher at advanced age stands (Figure 6C). Herein, because it is not convenient to show all the maps for the 50 stands, Figures 7 and 8 is showing as an example the predicted map of stem volumes and CV (%) with spatial resolution of 25 m for only three stands, but with ages ranging from three to nine years old.

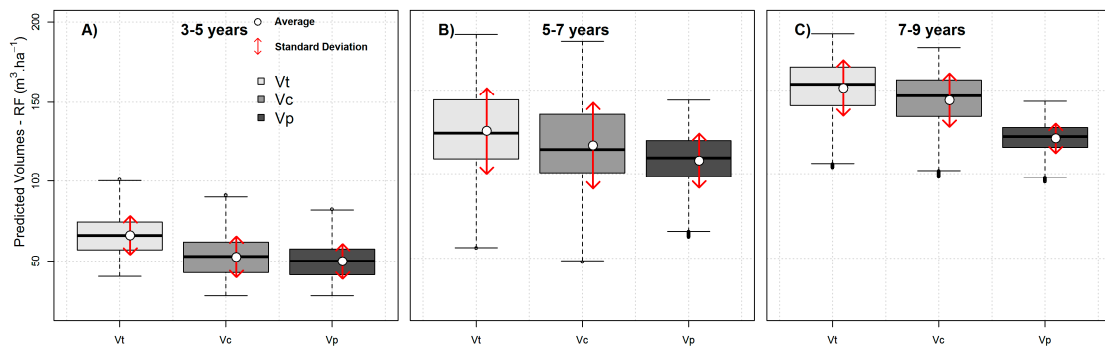


Figure 6. Predicted V_t , V_c and V_p of *P. taeda* at stand-level for the studied stands. (A) 3–5 years; (B) 5–7 years and (C) 7–9 years. The thick line in the box indicates the median value of the predicted stem volume. Boxes extend from the 25th to the 75th percentile, whiskers extend 1.5 times the length of the interquartile range above and below the 75th and 25th percentiles. The white dot is the mean of the predicted stem volume, and the vertical red lines represents the standard deviation around the mean (Mean \pm SD).

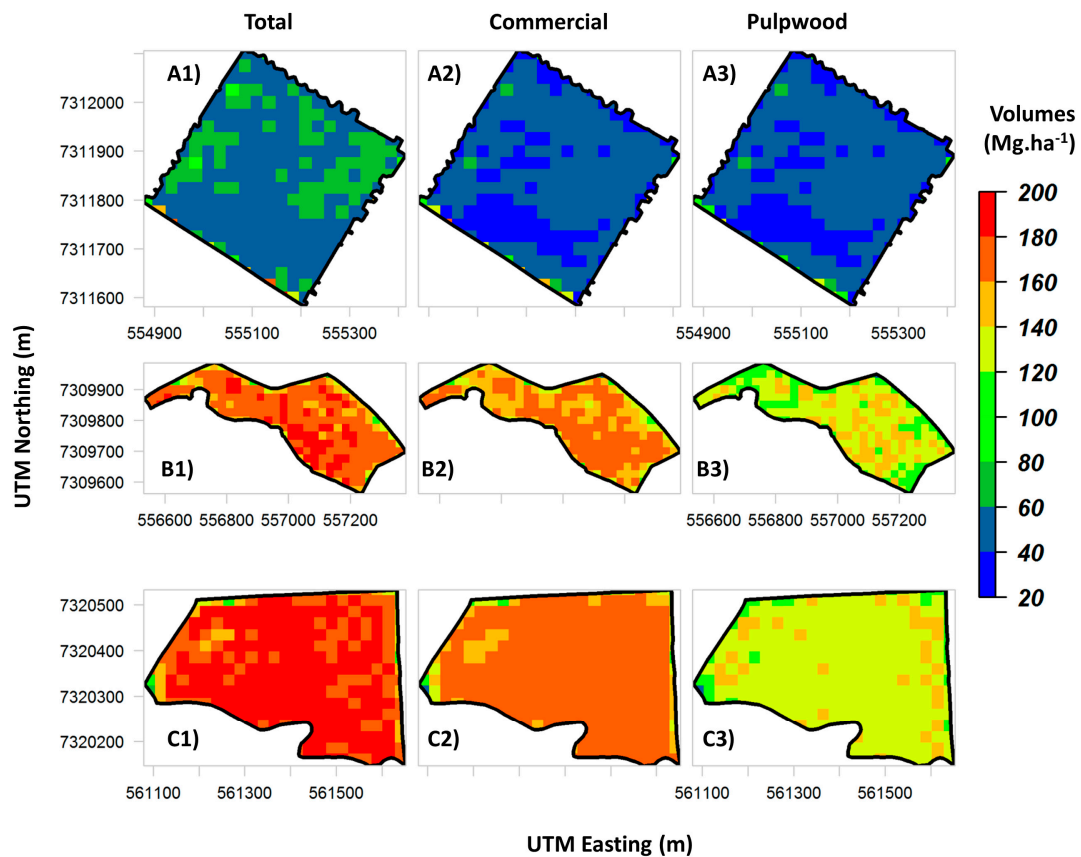


Figure 7. Predicted V_t (A1–C1), V_c (A2–C2) and V_p (A3–C3) of *P. taeda* at stand-level obtained from the RF models. Representative stand of early (i.e., 3–5 years) (A1–3), intermediate (i.e., 5–7 years) (B1–3) and advanced-stages of development (i.e., 7–9 years) (C1–3).

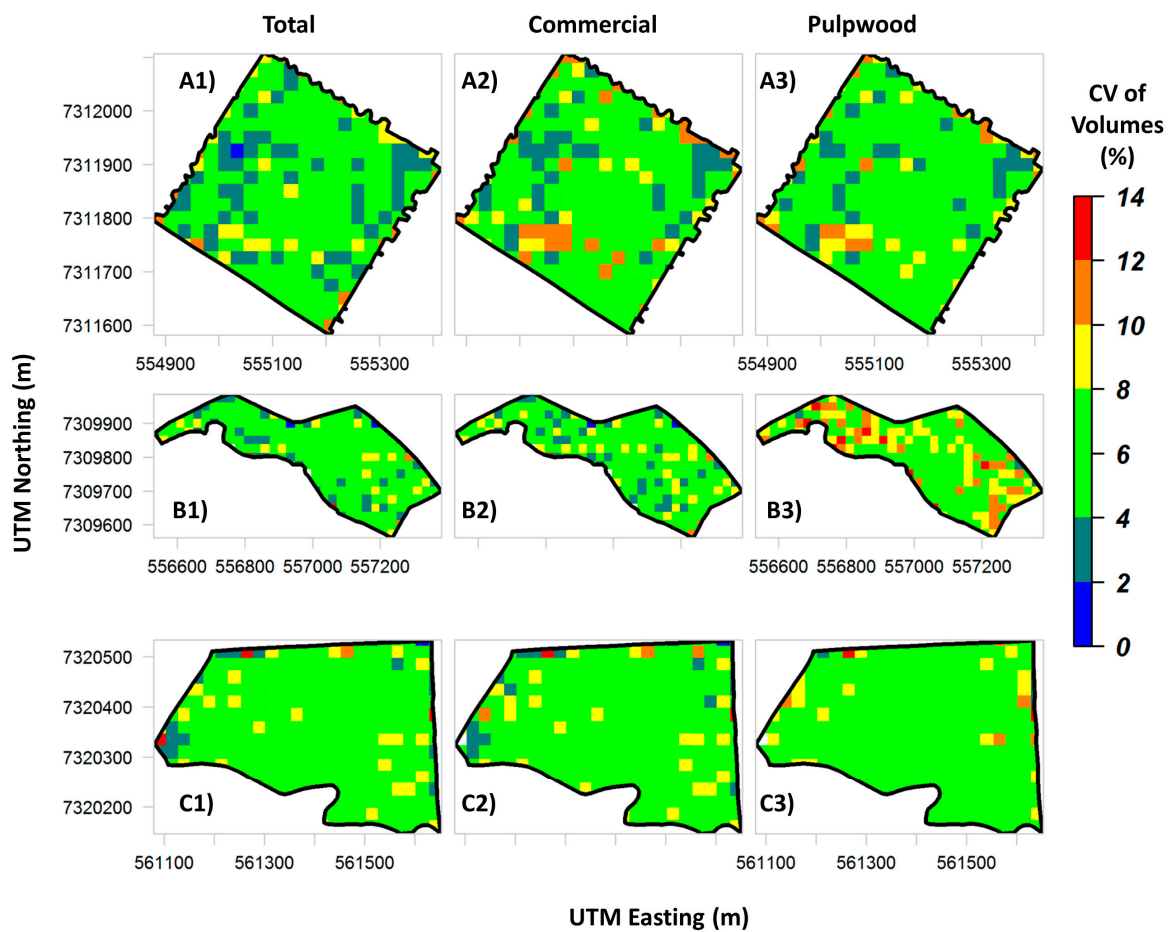


Figure 8. Coefficient of variation (CV) maps in percentage (%) of V_t (A1–C1), V_c (A2–C2) and V_p (A3–C3) of *P. taeda* at stand-level obtained from the 500 RF bootstrapped runs. Representative stand of early (i.e., 3–5 years) (A1–3), intermediate (i.e., 5–7 years) (B1–3) and advanced stages of development (i.e., 7–9 years) (C1–3).

4. Discussion

Detailed information on stem total and assortments volumes is required in industrial forest plantations to achieve production efficiency. For instance, incomplete or inaccurate forest information adds to the expense and challenge of forest operations (e.g., [42]). Moreover, improving forest plantation productivity and efficiency are important for reducing harvest pressure on natural forests. To achieve efficiency gains in operational forest management, a wide range of forest inventory attributes are required to be measured accurately at high spatial resolution and landscape to regional extents [34,43]. More detailed inventory information can allow forest owners to make better decisions concerning the timing of timber sales, and allow forest companies to optimize their wood supply chain from forest to factory [44]. In this study, we present a framework for predicting and mapping total, commercial and pulpwood volumes in industrial *P. taeda* forest plantations using airborne lidar data and RF. While there have been previous studies exploring the use of lidar and non-parametric machine learning algorithm for forest inventory modeling (e.g., [19,34,40,45–48]), no studies yet have demonstrated the potential of lidar and RF combined for predicting and mapping commercial and pulpwood volumes in industrial pine forest plantations.

Stem total and assortment volumes are directly related to the supply of fiber to pulp and paper companies. Herein, the accuracy of lidar for retrieving V_t , V_c and V_p using RF models was clearly demonstrated through achieving a relative RMSE and Bias less than <15% both for modeling and for

validation. As we are predicting forest attributes at a homogenous and single layered forest structure, our measures of precision and accuracy were similar to or higher than those who used lidar data for predicting stem volume through a RF framework in other forest types [15,16,42,44,49]. Among prior studies, RF has generally showed better performance compared to other statistical approaches, such as multiple linear regression, boosting trees regression and support vector regression [50–53]. Lidar-derived stem total and saw log volumes and their estimation accuracies have previously been reported at the forest stand level (e.g., [15,16,42,54,55]). For instance, in Eastern Finland in a typical Finnish southern boreal managed forest area, two studies used lidar data for estimating species-specific diameter distributions and saw log volumes [15,16]. Two years later, in Southern Wisconsin, USA, lidar data were used for predicting not only saw log volume, but also pulpwood volume [55]; the models produced R^2 of ~ 0.65 for estimating both saw log and pulpwood volumes. While those authors have showed the great potential of lidar in retrieving assortment volumes, this specific application is still relatively novel and further studies, such as presented herein, still need to be carried out.

In this study, we showed that lidar measurements could be used as input data to predict and map stem total and assortment volumes through a RF framework. High levels of accuracy were found when predicting V_t , V_c and V_p volumes across variable stand ages of *P. taeda* using only H99TH and HSKEW as predictor variables. Lidar-derived H99TH represents the top of the canopy (height at 99th percentile) and HSKEW is a measure of the asymmetry of height distribution, which is associated with the age of the stands because older trees are taller and cause a more positively skewed distribution. Skewness and height percentile variables are logical selections for distinguishing between different volume levels based on distributional shapes and height frequencies [56]. In particular, these variables can explain changes in the volume distribution [5], thus providing a solid justification for inclusion in the predictive model. Our results suggest that models based on variables describing the height of the canopy and the symmetry of the distribution of the returns are capable of predicting stem total and assortment volumes across different tree ages in industrial *P. taeda* forest plantations. Height percentile lidar metrics, such as H99TH, and height distributional metrics, such as HSKEW, have been shown to be powerful metrics for modeling and predicting forest attributes (e.g., [5–7,33,34,48]).

A disadvantage of using the RF framework presented here is that RF models do not extrapolate predictions beyond the trained data, and consequently, as found herein, reduce the variance compared to the observations (Figure 5). However, an important advantage of non-parametric approaches, such as RF, is that they can model non-linear, complex relationships between the dependent and the independent variables more efficiently than parametric approaches [46]. Furthermore, RF is insensitive to data skew, robust to a high number of variable inputs, and its implementation does not require pre-stratification by forest type [20,34,46]. From an overall statistical perspective, the predicted and observed volumes were equivalent, although our RF model validations showed a systematic tendency to overestimate small values and underestimate high values. The same was found in previous studies (e.g., [40,57]). According to one study [57], a possible cause might be that because the RF model estimates values by averaging the predictions of many decision trees, it might tend to underestimate when the predicted value is close to the maximum value of the training data. Similarly, when the estimated value is close to the minimum value of training data it might tend to overestimate. Other possible causes might be that we have a relatively small number of field plots, especially in the young and older stands.

Traditional forest inventory approaches are not effective in terms of costing and mobility especially in *P. taeda* forest plantations, where there is a need to monitor annual forest growth and properties are very large. Lidar remote sensing constitutes an important step towards operational wood procurement planning and is of high current interest to forestry organizations. Such technology is of great interest owing to their spatial sampling capabilities within plantations, and have had great reliability in forest inventory work in countries such as Norway, Canada, or the USA (e.g., [6,7,12,58]). Moreover, the application of airborne lidar technology for Brazilian industrial management is relatively new. While some studies have showed that the cost of the forest inventory derived from lidar could be lower than conventional forest inventory [59,60], the cost of lidar data acquisition could still be high

to monitor forest growth annually; however, lidar has the ability to provide wall-to-wall, accurate mapping of forest attributes at high spatial resolutions (e.g., Figures 7 and 8).

Traditional forest inventory approaches are based on sampling theory, and forest attributes measured at plot level are then used to infer inventory attributes for an entire stand [5,14]. We showed here that lidar and RF machine learning combined can be a powerful tool for mapping forest attributes in *P. taeda* forest plantations. In practice, lidar-derived maps of stem total and assortment volumes (Figures 7 and 8) allow the owners to evaluate the production and forest structure variability within stands in a spatially explicit manner, which is not possible in a traditional forest inventory of *P. taeda*. Also, such maps may allow managers to detect spatial patterns related to tree diseases, fire or forest clearing.

Recently, a study carried out in *Eucalyptus* spp. forest plantations showed that lidar and RF could be combined to predict and map aboveground carbon at high spatial resolution (5 m), even if the models are calibrated using field plots with area larger than the cell size used for mapping [34]. Therefore, future studies should be also test the ability of lidar and RF to map stem total and assortment volumes even at higher spatial resolution than presented in this study (e.g., Figures 7 and 8). Herein, we demonstrated the potential of combined lidar-derive metrics and RF to predict forest attributes through a lidar-plot based approach framework, however, to get even higher amount of details in *P. taeda* forest plantations, RF could be also tested in a lidar-individual tree based approach. For instance, RF has been successfully used to impute individual tree height and volume in longleaf pine (*Pinus palustris* Mill.) forest in Southern USA [61]; therefore, lidar and RF could be also used to predict stem total and assortment volumes at an individual tree level in *P. taeda* forest plantations, if carefully implemented.

5. Conclusions

Refining strategies for improving productivity of forest plantations requires accurate and detailed spatial information on forest structure and growing stock volume. In this study, we showed that airborne lidar data metrics can predict total, commercial and pulpwood volumes in a *P. taeda* forest plantation in Brazil. We found that different stem volumes can be estimated with high levels of accuracy from two lidar-derived variables describing the height and the shape of the vertical distribution of the height. The use of a model based on two variables suggests a higher generalization potential than models based on specific metrics that could result in over-fitting. However, this potential should be tested in other plantations and forested environments. Although airborne lidar data has not been adopted by paper companies operationally, our results show that the method used could be readily applied to support the supply chain of pulp and paper companies in Brazil or elsewhere.

Acknowledgments: This research was funded through a PhD scholarship from the National Council of Technological and Scientific Development (CNPq) via the Science without Borders Program (Process 249802/2013-9) and USDA Forest Service. The authors are very grateful for the lidar and field inventory data collections funded by Klabin S.A., a pulp and paper company. Mariano Garcia is supported by a Marie Curie International Outgoing Fellowship within the 7th European Community Framework Programme (ForeStMap—3D Forest Structure Monitoring and Mapping, Project Reference: 629376). The contents on this paper reflect only the authors' views and not the views of the European Commission. We thank three anonymous reviewers for their helpful suggestions on the first version of the manuscript.

Author Contributions: All the authors have made substantial contribution towards the successful completion of this manuscript. They all have been involved in designing the study, drafting the manuscript and engaging in critical discussion. C.A.S., C.K., A.T.H., L.A.V., W.S.W.M.J. and M.M., contributed with the methodological framework, data processing analysis and write up. M.G., A.F., A.C. and S.S. contributed to the interpretation, quality control and revisions of the manuscript. All authors read and approved the final manuscript.

Conflicts of Interest: The authors declare no conflict of interest.

References

1. Payn, T.; Carnus, J.-M.; Freer-Smith, P.; Kimberley, M.; Kollert, W.; Liu, S.; Orazio, C.; Rodriguez, L.; Silva, L.N.; Wingfield, M.J. Changes in planted forests and future global implications. *For. Ecol. Manag.* **2015**, *352*, 57–67. [[CrossRef](#)]

2. Indústria Brasileira de Árvores (IBÁ). Brazilian Tree Industry. 2015. Available online: http://www.iba.org/images/shared/iba_2015.pdf (accessed on 10 November 2016).
3. Kohler, S.V.; Wolff, N.I.; Figueiredo Filho, A.; Arce, J.E. Dynamic of assortment of *Pinus taeda* L. plantation in different site classes in Southern Brazil. *Sci. For.* **2014**, *42*, 403–410.
4. Silva, C.A.; Klauberg, C.; Hudak, A.T.; Vierling, L.A.; Liesenberg, V.; Bernett, L.G.; Scheraiber, C.F.; Schoeninger, E.R. Estimating Stand Height and Tree Density in *Pinus taeda* plantations using in-situ data, airborne LiDAR and k-Nearest Neighbor Imputation. *Ann. Braz. Acad. Sci.* **2017**, *90*, 1–15, in press.
5. Silva, C.A.; Klauberg, C.; Hudak, A.T.; Vierling, L.A.; Liesenberg, V.; Carvalho, S.P.; Rodriguez, L.C. A principal component approach for predicting the stem volume in *Eucalyptus* plantations in Brazil using airborne Lidar data. *Forestry* **2016**, *89*, 422–433. [[CrossRef](#)]
6. Næsset, E. Determination of mean tree height of forest stands using airborne laser scanner data. *ISPRS J. Photogramm.* **1997**, *52*, 49–56. [[CrossRef](#)]
7. Næsset, E. Predicting forest stand characteristics with airborne scanning laser using a practical two-stage procedure and field data. *Remote Sens. Environ.* **2002**, *80*, 88–99. [[CrossRef](#)]
8. Næsset, E.; Gobakken, T.; Holmgren, J.; Hyyppä, H.; Hyyppä, J.; Maltamo, M.; Nilsson, M.; Olsson, H.; Persson, Å.; Söderman, U. Laser scanning of forest resources: The Nordic experience. *Scand. J. For. Res.* **2004**, *19*, 482–499. [[CrossRef](#)]
9. Næsset, E. Airborne laser scanning as a method in operational forest inventory: Status of accuracy assessments accomplished in Scandinavia. *Scand. J. For. Res.* **2007**, *22*, 433–442. [[CrossRef](#)]
10. Hudak, A.T.; Evans, J.S.; Stuart, A.M. Lidar utility for natural resource managers. *Remote Sens.* **2009**, *1*, 934–951. [[CrossRef](#)]
11. Andersen, H.E.; McGaughey, R.J.; Reutebuch, S.E. Estimating forest canopy fuel parameters using lidar data. *Remote Sens. Environ.* **2005**, *94*, 441–449. [[CrossRef](#)]
12. Hudak, A.T.; Crookston, N.L.; Evans, J.S.; Falkowski, M.J.; Smith, A.M.; Gessler, P.E.; Morgan, P. Regression modeling and mapping of coniferous forest basal area and tree density from discrete-return lidar and multispectral satellite data. *Can. J. Remote Sens.* **2006**, *32*, 126–138. [[CrossRef](#)]
13. White, J.C.; Wulder, M.A.; Buckmaster, G. Validating estimates of merchantable volume from airborne laser scanning (ALS) data using weight scaled data. *For. Chron.* **2014**, *90*, 378–385. [[CrossRef](#)]
14. Silva, C.A.; Klauberg, C.; Carvalho, S.D.P.C.; Hudak, A.T. Mapping aboveground carbon stocks using Liar data in *Eucalyptus* spp. plantations in the state of São Paulo, Brazil. *Sci. For.* **2014**, *42*, 591–604.
15. Korhonen, L.; Peuhkurinen, J.; Jukka, M.; Suvanto, A.; Maltamo, M.; Packalen, P.; Kangas, J. The use of airborne laser scanning to estimate sawlog volumes. *Forestry* **2008**, *81*, 499–510. [[CrossRef](#)]
16. Peuhkurinen, J.; Maltamo, M.; Malinen, J. Estimating Species-Specific diameter distributions and saw log recoveries of boreal forests from airborne laser scanning data and aerial photographs: A distribution-based approach. *Silva Fenn.* **2008**, *42*, 600–625. [[CrossRef](#)]
17. Sherrill, J.R.; Bullock, B.P.; Mullin, T.J.; McKeand, S.E.; Purnell, R.C. Total and merchantable stem volume equations for mid rotation loblolly pine (*Pinus taeda* L.). *South. J. Appl. For.* **2011**, *35*, 105–108.
18. Hudak, A.T.; Crookston, N.L.; Evans, J.S.; Hall, D.E.; Falkowski, M.J. Nearest neighbor imputation of species-level, plot-scale forest structure attributes from lidar data. *Remote Sens. Environ.* **2008**, *112*, 2232–2245. [[CrossRef](#)]
19. Ahmed, O.S.; Franklin, S.E.; Wulder, M.A.; White, J.C. Characterizing stand-level forest canopy cover and height using landsat time series, samples of airborne lidar, and the random forest algorithm. *ISPRS J. Photogramm. Remote Sens.* **2015**, *101*, 89–101. [[CrossRef](#)]
20. Breiman, L. Random forests. *Mach. Learn.* **2001**, *45*, 5–32. [[CrossRef](#)]
21. Grossmann, E.; Ohmann, J.; Kagan, J.; May, H.; Gregory, M. Mapping ecological systems with a random forest model: Tradeoffs between errors and bias. *GAP Anal. Bull.* **2010**, *17*, 16–22.
22. Naidoo, L.; Cho, M.A.; Mathieu, R.; Asner, G. Classification of savanna tree species, in the Greater Kruger National Park region, by integrating hyperspectral and Lidar data in a Random Forest data mining environment. *ISPRS J. Photogramm. Remote Sens.* **2012**, *69*, 167–179. [[CrossRef](#)]
23. Yu, X.; Hyyppä, J.; Vastaranta, M.; Holopainen, M.; Viitala, R. Predicting individual tree attributes from airborne laser point clouds based on the random forests technique. *ISPRS J. Photogramm. Remote Sens.* **2011**, *661*, 28–37. [[CrossRef](#)]

24. Ko, C.; Sohn, G.; Rimmel, T.K.; Miller, J.R. Maximizing the Diversity of Ensemble Random Forests for Tree Genera Classification Using High Density Lidar Data. *Remote Sens.* **2016**, *8*, 646. [[CrossRef](#)]
25. Olden, J.D.; Lawler, J.J.; Poff, N.L. Machine learning methods without tears: A primer for ecologists. *Q. Rev. Biol.* **2008**, *83*, 171–193. [[CrossRef](#)] [[PubMed](#)]
26. Stumpf, A.; Kerle, N. Object-oriented mapping of landslides using Random Forests. *Remote Sens. Environ.* **2011**, *115*, 2564–2577. [[CrossRef](#)]
27. Lawrence, R.L.; Wood, S.D.; Sheley, R.L. Mapping invasive plants using hyperspectral imagery and Breiman Cutler classifications (RandomForest). *Remote Sens. Environ.* **2006**, *100*, 356–362. [[CrossRef](#)]
28. Köppen, W.; Geiger, R. *Klimakarte der Erde. Wall-Map 150 cm × 200 cm*; Verlag Justus Perthes: Gotha, Germany, 1928.
29. Curtis, R.O. Height-diameter and height-diameter-age equations for second-growth Douglas-fir. *For. Sci.* **1967**, *13*, 365–375.
30. Schöpfer, W. *Automatisierung Des Massem, Sorten Und Wertberechnung Stenender Waldbestande Schriftenreihe Bad; Wurt-Forstl: Koblenz, Germany, 1966.*
31. McGauchey, R.J. *FUSION/LDV: Software for LiDAR Data Analysis and Visualization*; Forest Service Pacific Northwest Research Station USDA: Seattle, WA, USA, 2015. Available online: <http://forsys.cfr.washington.edu/fusion/FUSIONmanual.pdf> (accessed on 15 October 2015).
32. Kraus, K.; Pfeifer, N. Determination of terrain models in wooded areas with airborne laser scanner data. *ISPRS J. Photogramm. Remote Sens.* **1998**, *53*, 193–203. [[CrossRef](#)]
33. Hudak, A.T.; Strand, E.K.; Vierling, L.A.; Byrne, J.C.; Eitel, J.U.H.; Martinuzzi, S.; Falkowski, M.J. Quantifying aboveground forest carbon pools and fluxes from repeat LiDAR surveys. *Remote Sens. Environ.* **2012**, *123*, 25–40. [[CrossRef](#)]
34. Silva, C.A.; Hudak, A.T.; Klauber, C.; Vierling, L.A.; Gonzalez-Benecke, C.; de Padua Chaves Carvalho, S.; Rodriguez, L.C.E.; Cardil, A. Combined effect of pulse density and grid cell size on predicting and mapping aboveground carbon in fast-growing Eucalyptus forest plantation using airborne LiDAR data. *Carbon Balance Manag.* **2017**, *12*, 13. [[CrossRef](#)] [[PubMed](#)]
35. Evans, J.S.; Cushman, S.A. Gradient modeling of conifer species using Random Forests. *Landsc. Ecol.* **2009**, *5*, 673–683. [[CrossRef](#)]
36. Evans, J.S.; Murphy, M.A.; Holden, Z.A.; Cushman, S.A. Modeling species distribution and change using Random Forests. In *Predictive Modeling in Landscape Ecology*; Drew, C.A., Huettmann, F., Wiersma, Y., Eds.; Springer: New York, NY, USA, 2010; pp. 139–159.
37. Liaw, A.; Wiener, M. *RandomForest: Breiman and Cutler's Random Forests for Classification and Regression, Version 4.6–12*. 2015. Available online: <https://cran.rproject.org/web/packages/randomForest/> (accessed on 15 October 2016).
38. R Core Team. *R: A Language and Environment for Statistical Computing*; R Foundation for Statistical Computing: Vienna, Austria, 2017. Available online: <http://www.R-project.org> (accessed on 20 October 2016).
39. Bright, B.C.; Hudak, A.T.; McGauchey, R.; Andersen, H.E.; Negron, J. Predicting live and dead tree basal area of bark beetle affected forests from discrete-return lidar. *Can. J. Remote Sens.* **2013**, *39*, S99–S111. [[CrossRef](#)]
40. Lopatin, J.; Dolos, K.; Hernández, H.J.; Galleguillos, M.; Fassnacht, F.E. Comparing Generalized Linear Models and random forest to model vascular plant species richness using LiDAR data in a natural forest in central Chile. *Remote Sens. Environ.* **2016**, *173*, 200–210. [[CrossRef](#)]
41. Robinson, A.P.; Duursma, R.A.; Marshall, J.D. A regression-based equivalence test for model validation: Shifting the burden of proof. *Tree Physiol.* **2005**, *25*, 903–913. [[CrossRef](#)] [[PubMed](#)]
42. Holopainen, M.; Vastaranta, M.; Rasinmäki, J.; Kalliovirta, J.; Mäkinen, A.; Haapanen, R.; Melkas, T.; Yu, X.; Hyypä, J. Uncertainty in timber assortment estimates predicted from forest inventory data. *Eur. J. For. Res.* **2010**, *129*, 1131–1142. [[CrossRef](#)]
43. Sibona, E.; Vitali, A.; Meloni, F.; Caffo, L.; Dotta, A.; Lingua, E.; Motta, R.; Garbarino, M. Direct Measurement of Tree Height Provides Different Results on the Assessment of LiDAR Accuracy. *Forests* **2017**, *8*, 7. [[CrossRef](#)]
44. Kankare, V.; Vauhkonen, J.; Tanhuanpaa, T.; Holopainen, M.; Vastaranta, M.; Joensuu, M. Accuracy in estimation of timber assortments and stem distribution—A comparison of airborne and terrestrial laser scanning techniques. *ISPRS J. Photogramm. Remote Sens.* **2014**, *97*, 89–97. [[CrossRef](#)]
45. Zhao, K.; Popescu, S.; Meng, X.; Pang, Y.; Agca, M. Characterizing forest canopy structure with lidar composite metrics and machine learning. *Remote Sens Environ.* **2011**, *115*, 1978–1996. [[CrossRef](#)]

46. Mascaro, J.; Asner, G.P.; Knapp, D.E.; Kennedy-Bowdoin, T.; Martin, R.E.; Anderson, C.; Higgins, M.; Chadwick, K.D. A tale of two “forests”: Random forest machine learning AIDS tropical forest carbon mapping. *PLoS ONE* **2014**, *9*, e85993. [[CrossRef](#)] [[PubMed](#)]
47. García Gutiérrez, J.; Martínez Álvarez, F.; Troncoso Lora, A.; Riquelme Santos, J.C. A comparison of machine learning regression techniques for LiDAR-derived estimation of forest variables. *Neurocomputing* **2015**, *167*, 24–31. [[CrossRef](#)]
48. Hudak, A.T.; Bright, B.C.; Pokswinski, S.M.; Loudermilk, E.L.; O’Brien, J.J.; Hornsby, B.S.; Klauberg, C.; Silva, C.A. Mapping forest structure and composition from low-density LiDAR for informed forest, fuel, and fire management at Eglin Air Force Base, Florida, USA. *Can. J. Remote Sens.* **2016**, *42*, 411–427. [[CrossRef](#)]
49. Hayashi, R.; Weiskittel, A.; Sader, S. Assessing the feasibility of low-density lidar for stand inventory attribute predictions in complex and managed forests of Northern Maine, USA. *Forests* **2014**, *5*, 363–383. [[CrossRef](#)]
50. Kankare, V.; Vastaranta, M.; Holopainen, M.; Raty, M.; Yu, X.; Hyypä, J.; Hyypä, H.; Alho, P.; Viitala, R. Retrieval of forest aboveground biomass and stem volume with airborne scanning LiDAR. *Remote Sens.* **2013**, *5*, 2257–2274. [[CrossRef](#)]
51. Wu, J.; Yao, W.; Choi, S.; Park, T.; Myneni, R.B. A Comparative Study of Predicting DBH and Stem Volume of Individual Trees in a Temperate Forest Using Airborne Waveform LiDAR. *IEEE Geosci. Remote Sens. Lett.* **2015**, *12*, 2267–2271. [[CrossRef](#)]
52. Shataee, S.; Weinaker, H.; Babanejad, M. Plot-level Forest Volume Estimation Using Airborne Laser Scanner and TM Data, Comparison of Boosting and Random Forest Tree Regression Algorithms. *Procedia Environ. Sci.* **2011**, *7*, 68–73. [[CrossRef](#)]
53. Peuhkurinen, J.; Maltamo, M.; Malinen, J.; Pitkänen, J.; Packalén, P. Pre-harvest measurement of marked stands using airborne laser scanning. *For. Sci.* **2007**, *53*, 653–661.
54. Holmgren, J.; Barth, A.; Larsson, H.; Olsson, H. Prediction of stem attributes by combining airborne laser scanning and measurements from harvesters. *Silva Fen.* **2012**, *46*, 227–239. [[CrossRef](#)]
55. Hawbaker, T.J.; Gobakken, T.; Lesak, A.; Trømborg, E.; Contrucci, K.; Radeloff, V. Light detection and ranging-based measures of mixed hardwood forest structure. *For. Sci.* **2010**, *56*, 313–326.
56. Van Aardt, J.A.N.; Wynne, R.H.; Oderwald, R.G. Forest Volume and Biomass Estimation Using Small-Footprint Lidar Distributional Parameters on a Per-Segment Basis. *For. Sci.* **2006**, *52*, 636–649.
57. Ota, T.; Ahmed, O.S.; Franklin, S.E.; Wulder, M.A.; Kajisa, T.; Mizoue, N. Estimation of Airborne Lidar Derived Tropical Forest Canopy Height Using Landsat Time Series in Cambodia. *Remote Sens.* **2014**, *6*, 10750–10772. [[CrossRef](#)]
58. Coops, N.C.; Hilker, T.; Wulder, M.A.; St-Onge, B.; Newnham, G.; Siggins, A. Estimating canopy structure of Douglas-fir forest stands from discrete-return lidar. *Trees* **2007**, *21*, 295–310. [[CrossRef](#)]
59. Tilley, B.K.; Munn, I.A.; Evans, D.L.; Parker, R.C.; Roberts, S.D. Cost Considerations of Using Lidar for Timber Inventory. 2004. Available online: <http://sofew.cfr.msstate.edu/papers/0504tilley.pdf/> (accessed on 21 March 2016).
60. Hummel, S.; Hudak, A.T.; Uebler, E.H.; Falkowski, M.J.; Megown, K.A. A comparison of accuracy and cost of LiDAR versus stand exam data for landscape management on the Malheur national forest. *J. For.* **2011**, *109*, 267–273.
61. Silva, C.A.; Hudak, A.T.; Vierling, L.A.; Loudermilk, E.L.; O’Brien, J.J.; Hiers, J.K.; Jack, S.B.; Gonzalez-Benecke, C.A.; Lee, H.; Falkowski, M.J.; et al. Imputation of individual longleaf pine forest attributes from field and LiDAR data. *Can. J. Remote Sens.* **2016**, *42*, 554–573. [[CrossRef](#)]

